Effect of Scale of Operation on CSD Dynamics in Evaporative Crystallizers

Johan Jager, Herman J. M. Kramer, Brian Scarlett, and Esso J. de Jong
Delft University of Technology, Laboratory for Process Equipment, Delft, The Netherlands

Sjoerd de Wolf
Delft University of Technology, Laboratory for Measurement & Control, Delft, The Netherlands

Experimental measurements of the crystal-size distribution (CSD) clearly indicate a pronounced difference in the dynamic behavior of a 20- and 970-L continuous crystallizer that produces ammonium sulfate. The difference in their circulation time offers a probable explanation for this phenomenon. It causes different supersaturation profiles in the two crystallizers, which leads to internal fines dissolution in the large crystallizer. This contributes to the observed oscillations in the 970-L crystallizer as opposed to the first-order responses in the 20-L crystallizer. To numerically study the effect of the supersaturation profile a dynamic model, from which the MSMPR (mixed suspension mixed product removal) assumption is omitted, is developed. Calculated supersaturation profiles differ considerably for the 20-L, the 970-L and an imaginary 50,000-L continuous evaporative crystallizer. Coincident with changes in the supersaturation profiles, the numerical solution of the model indicates the tendency of large crystallizers to oscillate and supports this suggested explanation.

I. Experimental

Introduction

Industrial crystallizers are known to exhibit large variations in the crystal-size distribution (CSD) they produce. These variations most probably result from unstable behavior of the crystallization process itself, although the influence of unwanted changes in process conditions cannot be fully excluded. Laboratory crystallizers, on the other hand, usually demonstrate stable operation that is illustrated by rapidly decaying CSD-transients (Randolph and Larson, 1988). Relatively few experimental studies have been devoted to the dynamic behavior of crystallizers in general, particularly to the difference in dynamic behavior between the crystallizers of different scale.

It was shown previously (Jager et al., 1990a,b) that CSD transients in a 20-L crystallizer rapidly approach steady-state conditions. These results can be simulated well with an MSMPR model including secondary nucleation kinetics combined with attrition. In this article, this analysis is made to a larger-scale of operation. Also discussed are CSD transients measured in a 970-L crystallizer, which was operated with and without fines removal and whose results are compared with CSD transients measured in the 20-L crystallizer, operated at the same conditions using the same ammonium sulfate solution. Finally, differences between the two crystallizers are explained.

Experimental Procedure

The 20-L crystallizer is a continuous, evaporative, draft-tube crystallizer, operated at 50°C. The crystallizer has a propeller stirrer of 100-mm-diameter operated at 700 rpm. Other dimensions, together with a process scheme, are given by Jager (1990). The slurry circulation time is approximately 2 seconds, equally divided between the inner and the outer tube. In this article, the crystallizer startup, at the operating conditions of the 970-L crystallizer, will be discussed. Sieve analysis of filtered and dried samples, using 20 Veco microprecision sieves, was used to measure CSD transients.

The continuous 970-L crystallizer is a draft-tube crystallizer that can be operated with and without fines removal. Its dimensions are given by Jager (1990). It has a 485-mm rubber-coated propeller and an internal heat exchanger, through which heat for evaporation is supplied or heat is removed in the case of cooling crystallization. The residence times in the outer and

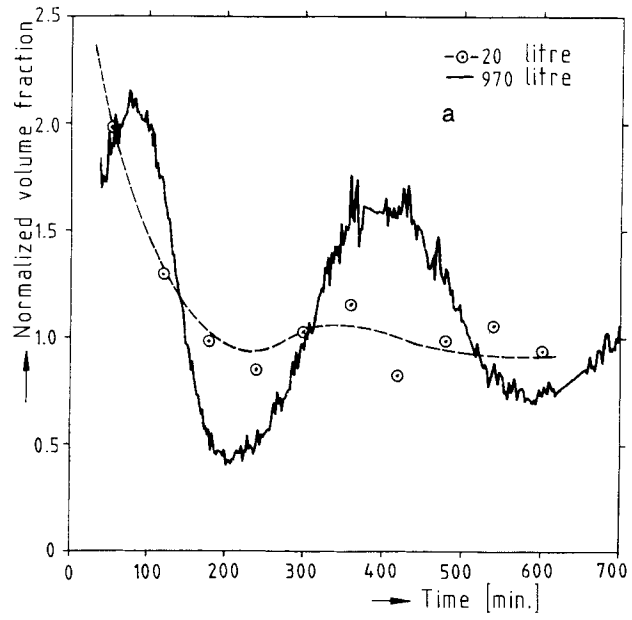

a. Size intervals 352–419 μm and 400–500 μ

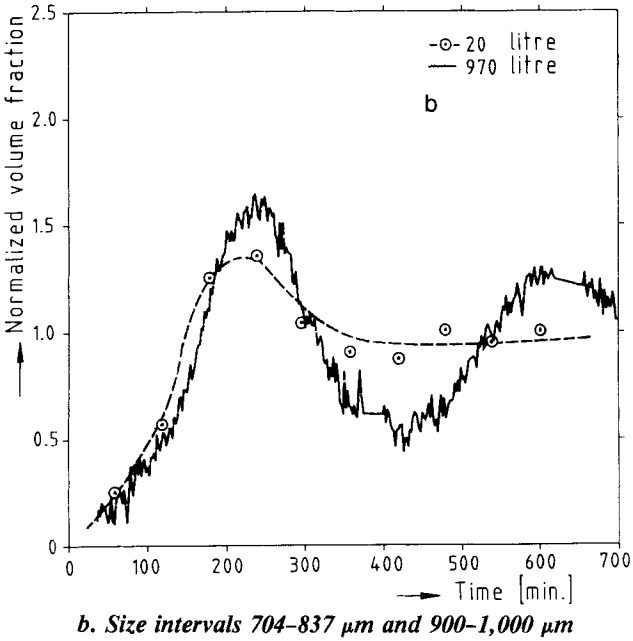

b. Size intervals 704–837 μm and 900–1,000 μm

Figure 1. Volume fractions normalized on end values.

Measured by sieve analysis in the 20-L crystallizer and Malvern analysis in the 970-L crystallizer during startup when operated without fines removal as an evaporative crystallizer

inner tube are approximately 7 and 6 seconds, respectively, at a stirrer speed of 314 rpm.

The product is removed through a smooth-shaped discharge in the outer tube. The discharge diameter is chosen to ensure isokinetic withdrawal, and the operating temperature is 50°C. CSD transients are monitored using a dilution unit, which samples and dilutes a product sample every 2 minutes in combination with a Malvern particle sizer that measures the size distribution in the diluted sample. The solids concentration is measured by densitometry using an Endress and Hauser M-point mass-flow densitometer. More details about the measurement technique are given by Jager et al. (1990c). The product flow, after dissolution, is reused as feed supply. Fines can be removed from an annular zone and dissolved or recycled in a fines processing system.

Experimental Results

Both crystallizers were operated at a residence time of 4,500 seconds and a heat input of 100 kW/m^3. Figure 1a shows the trends during startup for comparable volume fractions in the size interval 352–419 μm for the 20-L crystallizer and the size interval 400–500 μm for the 970-L crystallizer. Figure 1b shows the comparable size intervals, 704–837 μm and 900–1,000 μm. Figure 2 shows the mass-based average size (m_4/m_3) for both runs. The responses are normalized on their end-values. The responses for the 20-L crystallizer are similar to those obtained previously at a residence time of 2,400 seconds. Both Figures 1 and 2 show a distinct difference in the shape of the responses. The 20-L crystallizer approaches the steady state, whereas the 970-L crystallizer shows severe oscillations. A comparison between sieve and Malvern analysis (Jager et al., 1990c) illustrates the significance of these differences.

What is remarkable, however, is the small difference in the average value for the mass-based size. Figures 3 and 4 show the same transients in the 970-L crystallizer for two volume fractions (400–500 μm and 900–1,000 μm) and the mass-based average size (m_4/m_3), respectively, over a longer period of time. Figures 5 and 6 show the same results for cooling crystallization, where a solution saturated at 75°C, is cooled down to 50°C at a residence time of 4,500 seconds. These results indicate a reduction in the number, as well as the amplitude, of the oscillations. Some transient behavior is, however, observed. Most probably, this is inherent in the process of startup, which

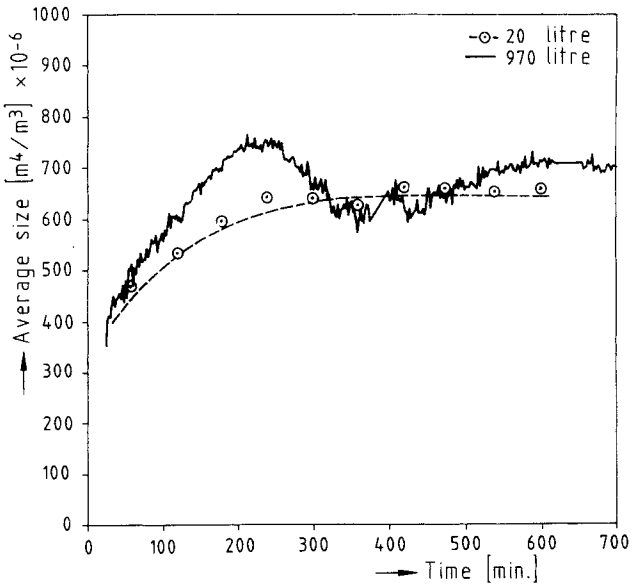

Figure 2. Mass-based average size.

Measured by sieve analysis in the 20-L crystallizer and by Malvern analysis in the 970-L crystallizer during startup when operated without fines removal as an evaporative crystallizer

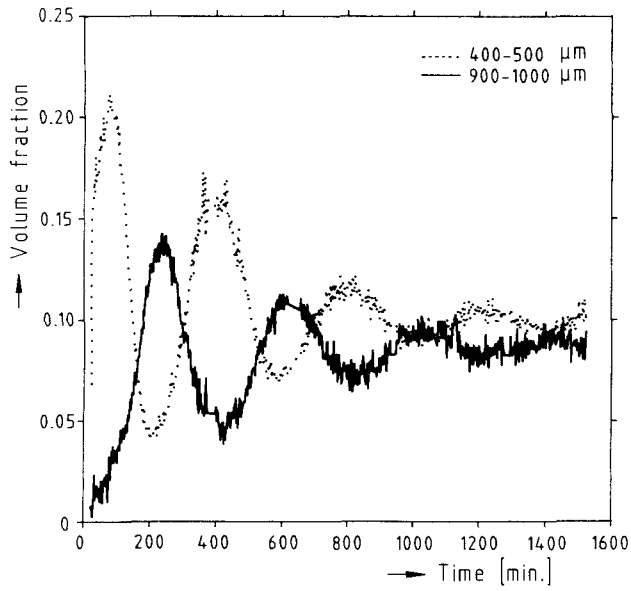

Figure 3. Volume densities for size intervals 400-500 μm and 900-1,000 μm.

During startup of the 970-L crystallizer when operated without fines removal as an evaporative crystallizer

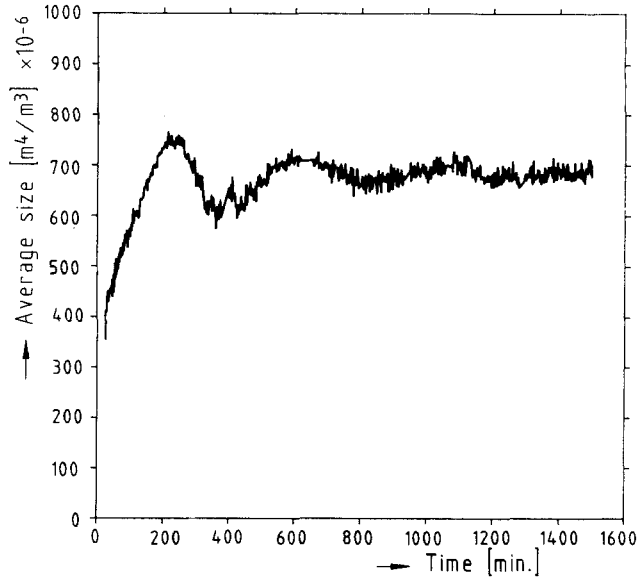

Figure 4. Mass-based average size.

During startup of the 970-L crystallizer when operated without fines-removal as an evaporative crystallizer

is always accompanied by an initial burst of nuclei, and thus some transient behavior. The effect of fines removal at a rate of 1.6 L/s for the volume fractions (400-500 μm) and (900-1,000 μm), and the mass-based average size are given in the Figures 7 and 8. The heat input and residence time were identical to the previous evaporative run. During a time of 1,000-1,400 min, the measurement technique was inactive in this run. These results indicate that fines removal tends to promote the tendency to oscillate.

Discussion

The tendency of the large crystallizer to oscillate, as opposed to the decaying transients in the 20-L crystallizer, requires an explanation. Previously, the occurrence of CSD oscillations was attributed to extremely nonlinear nucleation kinetics (sodium chloride-ethanol-water) (Yu and Douglas, 1975), such as Miers kinetics and secondary nucleation kinetics that contain a threshold value for the supersaturation before nucleation occurs (magnesium sulfate-water) (Ottens, 1973):

$$B = k_b\,(C^* - C_0^*)^i\, m_j^k \quad \text{if } C^* \geqq C_0^*$$

$$B = 0 \quad \text{if } C^* \leqq C_0^*$$

where

B = nucleation rate
m_j = jth moment of the CSD
C^* = supersaturation
C_0^* = minimum supersaturation before nucleation occurs
k_b = nucleation constant

Simulated responses using these nucleation kinetics indeed show CSD-oscillations, when the crystallizer is operated in the vicinity of C_0^* (Ottens, 1973; Yu and Douglas, 1975). Others (Beckman and Randolph, 1977; Aeschbach and Bourne, 1972; Aeschbach and Bourne, 1979) found that product classification may enhance crystallizer instability.

A change in the scale of operation from 20 to 970 L is not likely to affect the nucleation kinetics to such an extent that oscillatory behavior is provoked. Besides, product classification is not used. The threshold-value theory is also disapproved by the increase in the number and amplitude of the oscillations when fines removal is applied. The effect of fines removal,

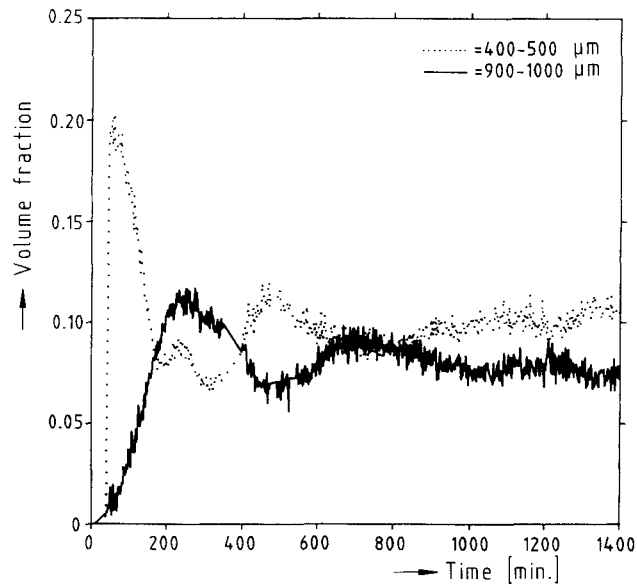

Figure 5. Volume densities for size intervals 400-500 μm and 900-1,000 μm.

During startup of the 970-L crystallizer when operated without fines removal as a cooling crystallizer

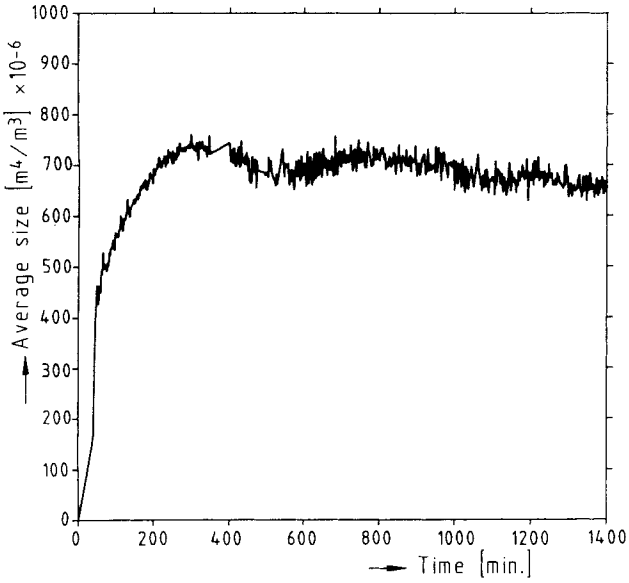

Figure 6. Mass-based average size.

During startup of the 970-L pilot-plant crystallizer when operated without fines-removal as a cooling crystallizer

assuming a well mixed crystallizer, is an increase in the average supersaturation that would move the process away from a low threshold value. Therefore, both explanations are unlikely to hold in this application, which requires a new hypothesis.

This hypothesis should explain a difference in CSD dynamics, rather than that in steady-state values that excludes simple changes in the nucleation rate, which was the thesis of previous scale-up studies (Grootscholten et al., 1984). Apart from the radial stirrer speed, the most predominant difference between draft-tube crystallizers of different scale is that in the circulation time, which affects the existing supersaturation profile. In an evaporative crystallizer, such a profile exists since supersaturation is created in the boiling zone. In scale-up, usually the height of the crystallizer will increase. Consequently, the

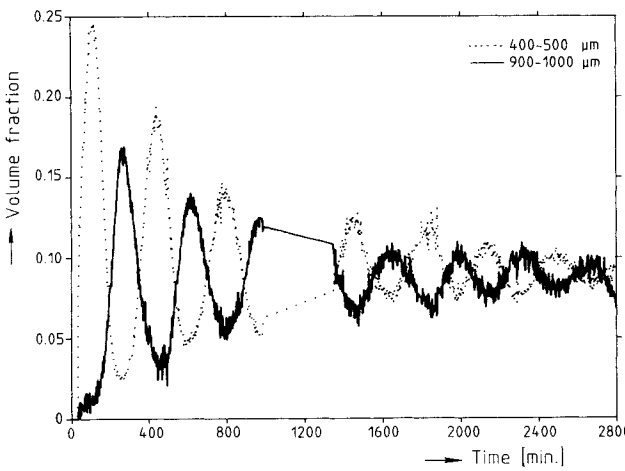

Figure 7. Volume densities for size intervals 400-500 μm and 900-1,000 μm.

During startup of the 970-L crystallizer when operated with fines removal as an evaporative crystallizer

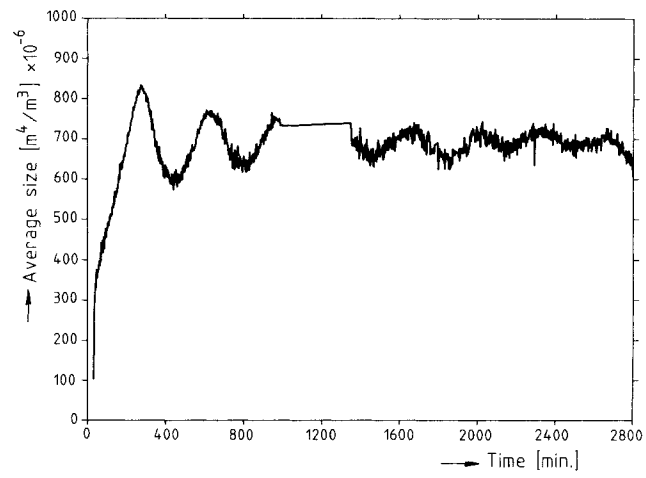

Figure 8. Mass-based average size.

During startup of the 970-L pilot-plant crystallizer when operated with fines-removal as an evaporative crystallizer

circulation time increases at a constant slurry velocity. This has two major effects.

1. It increases the time available for desupersaturation.
2. It increases the rise in supersaturation in the boiling zone.

They occur because the ratio between the evaporation rate and the circulation rate increases at a constant production rate per cubic meter crystallizer. A small-scale crystallizer has a short circulation time and is, therefore, most probably supersaturated over its entire volume. A large-scale crystallizer, on the other hand, may have positions that are undersaturated where the undersaturated feed enters the crystallizer or in a heat exchanger where the heat is supplied for evaporation. This change in profile certainly affects the CSD through changes in the ratio between crystal growth and nucleation. However, it also opens up the possibility of internal fines dissolution occurring by a mechanism discussed in Part II on the Model Approach. This phenomenon can be the source of crystallizer instability. This is supported by the observation that cooling crystallization reduces the number and amplitude of the oscillations. In cooling crystallization undersaturation, and thus internal fines dissolution, is avoided if the feed flow is saturated.

Another source of crystallizer instability has recently been suggested by Randolph and Larson (1988). They postulated an upper level of supersaturation where a rapid increase in the nucleation rate occurs as a result of homogeneous nucleation. High levels of supersaturation can indeed exist in the boiling zone of a large-scale crystallizer, as will be illustrated in Part II. However, at the high degree of desupersaturation for a fast-growing system, the supersaturation in the boiling zone is relatively invariant with time because it is mainly determined by the evaporation rate and the circulation rate. Therefore, its primary importance as a source of the oscillations must be questioned.

Conclusions

The experimental data indicate a significant change in the CSD dynamics with a change in the scale of operation. This

suggests that a scale effect should be included in the dynamic model of a continuous evaporative crystallizer to account for these differences. A change in the supersaturation profile with the scale of operation has been identified as a possible explanation for the observed changes. To substantiate this hypothesis, the mixed suspension assumption is rejected and an extended model, which includes a supersaturation profile, is developed next.

II. Model Approach

Introduction

The experimental data have indicated the necessity to account for the supersaturation profile in a crystallizer. In evaporative crystallizers, supersaturation is created in the boiling zone and subsequently depleted while the slurry circulates down the crystallizer and up the draft-tube. This creates a supersaturation profile which, by assuming that the crystallizer is well mixed, is generally neglected. Three exceptions were found: Wiker and Anshus (1974), Grootscholten and De Jong (1979), and Kratz and Hoyer (1989) who studied the steady-state effects of such a profile. In this part of the article, an attempt is made to establish a new dynamic model, in which the well mixed assumption is avoided. In this simplified model, the crystallizer is divided into three sections: 1. the boiling zone, 2. the outer draft tube where the slurry is always supersaturated, and 3. the inner draft tube where the slurry can be either supersaturated or undersaturated. Also discussed are a population balance, a heat balance, mass balances, and rate equations. The set of equations is numerically solved for a 20, a 970 and a 50,000-L continuous, evaporative crystallizer.

Theory

The crystallizer is divided into three interconnected sections, Figure 9.

1. *Boiling Zone.* Supersaturation is created in the boiling zone. This zone has no volume and acts as a junction, where the feed flow, the product flow, the vapor flow, and two internal flows interconnect. The feed flow mixes with the internal flow and relieves the heat, which was introduced in the internal exchanger by evaporation. This increases the concentration and decreases the saturation concentration, as a result of the drop in temperature in the boiling zone, in the internal stream which then enters the second section (the outer draft tube).

2. *Outer Draft Tube.* In the outer draft tube, the supersaturation is depleted by deposition on the available crystal surface while the slurry travels down the draft tube. The draft tube is considered to be an idealized plug flow reactor with no axial dispersion. If fines removal is employed, fines are removed at the bottom of the outer tube assuming a perfect separation at a cutsize (L_{fi}), instantly dissoluted, and returned as solute to the internal stream. Crystal growth and crystal birth continue until the slurry enters the internal heat exchanger, which marks the third section (the inner draft tube).

3. *Inner Draft Tube.* In the internal heat exchanger located at the lower end of the inner draft tube, the temperature is raised instantly. This increases the saturation concentration and can reverse the supersaturation to undersaturation. If the slurry remains supersaturated, crystal growth continues. Otherwise, crystal dissolution commences and continues until the boiling zone is reentered.

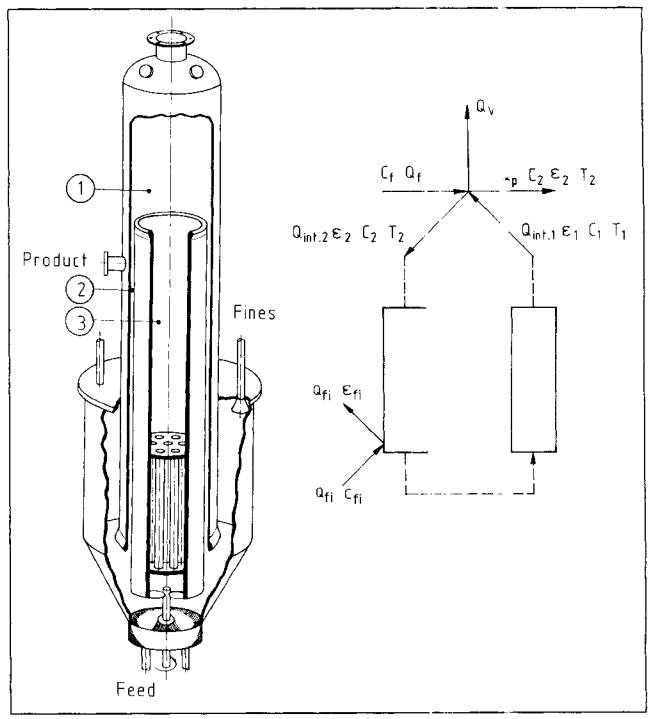

Figure 9. 970-L crystallizer and simplified model.

For simplicity, only the most important features are included in the model. It can include axial flow dispersion by introducing an axial flow diffusivity (Riviera and Randolph, 1978), by defining a fines classification function instead of a sharp cut at L_{fi}, or by adding a mixing compartment in the boiling zone, the effect of which was investigated at steady-state conditions by Wiker and Anshus (1974).

To simulate the CSD dynamics over these sections, an infinitesimally small volume of slurry is pursued while it travels through the crystallizer, and the population balance is solved for this volume only. The slip velocity of the crystals is neglected, and thus the crystals stay in one specific lump of slurry. The inner and outer draft tubes act as a plug flow reactor. Crystals are removed as product when the element passes the boiling zone or as fines when they pass the fines draw-off position.

Balances

Boiling zone

Heat and mass balances over the boiling zone, together with a heat balance that determines the raise in temperature in the internal heat exchanger, are discussed in the Appendix. Using these balances, the solute concentration and solids concentration in the internal stream, which leaves the boiling zone, can be calculated. The decrease in population density, caused by product removal in the boiling zone, is given by:

$$\frac{n_2\ (L,\ t)}{n_1\ (L,\ t)} = \frac{[1\ -\ \epsilon_2(t)]}{[1\ -\ \epsilon_1(t)]} \tag{1}$$

where

$\epsilon(t)$ = the void fraction $[1 - k_v m_3(t)]$.

Crystallizer internal: supersaturated

The distribution of crystals over size can be modeled using the population balance approach. If crystal breakage and agglomeration are neglected, and crystals are assumed to form at a very small size, the population balance for a volume of slurry moving with a constant velocity in a plug flow reactor is given by (Randolph and Larson, 1988):

$$\frac{\partial n(L, t)}{\partial t} + \frac{\partial [G(L, t)\, n(L, t)]}{\partial L} = 0 \tag{2}$$

where

$n(L, t)$ = population density at size L
$G(L, t)$ = growth rate at size L

The boundary condition for this hyperbolic partial differential equation is given by:

$$n_0(t) = \frac{B(t)}{G(L_0, t)} \tag{3}$$

where

$B(t) = k_b C^*(t)^i m_j(t)^k$ power law for the nucleation rate B
$n_0(t)$ = population density at very small size
k_b, i, j, k = empirical constants

The moments of distribution (m_j) are defined by:

$$m_j = \int_0^\infty n(L, t)\, L^j\, dL \tag{4}$$

The crystal growth process, presented here by the linear growth rate G, can usually be considered as a two-stage process: a) diffusive convective mass transfer from the bulk of the solution to the crystal surface; and b) incorporation in the crystal lattice, Figure 10. The driving force for diffusive, convective mass transfer is the difference between the bulk concentration (C_b) and the concentration at the crystal-interface (C_{if}):

$$R = k_d\, (C_b - C_{if}) \tag{5}$$

The driving force for the incorporation in the crystal lattice is the difference between the concentration at the interface and the saturation concentration (C_s), which in terms of mass fluxes can be presented by:

$$R = k_r\, (C_{if} - C_s)^r \tag{6}$$

Assuming that the surface integration is first-order dependent on the supersaturation ($r = 1$), the growth rate is given by Eq. 7 using an overall mass transfer coefficient given by Eq. 8.

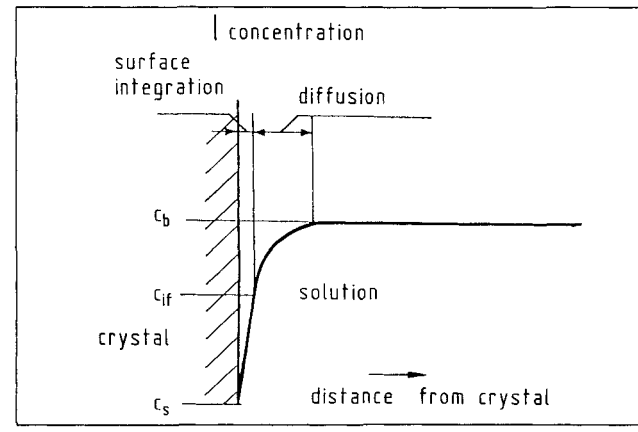

Figure 10. Mass transfer to a growing crystal.

$$G(L, t) = k_g(L)\, \frac{k_a}{3\, k_v\, \rho_c}\, C^*(t) \tag{7}$$

$$\frac{1}{k_g(L)} = \frac{1}{k_d(L)} + \frac{1}{k_r} \tag{8}$$

where

$k_d(L)$ = mass transfer coefficient for diffusion
k_r = surface reaction constant
k_a = surface of a crystal of size L/L^2
k_v = volume of a crystal of size L/L^3
$C^*(t) = C_b(t) - C_s(T_2)$ (9)

Crystals diminish in size as a result of crystal attrition. Crystal attrition, modeled according to an attrition rate (G_a), has been related to the third moment of the crystal size distribution and the crystal size (Jager et al., 1990b). An overall relation for the crystal growth rate finally results.

$$G_a\, (L, t) = a\, m_3(t)\, (L - L_a)^b \tag{10}$$

where

a = a negative rate constant
L_a = minimum size for attrition
b = empirical constant

$$G(L, t) = k_g(L)\, \frac{k_a}{3\, k_v\, \rho_c}\, C^*(t) + G_a(L, t) \tag{11}$$

The available supersaturation is reduced by the crystal growth according to a concentration balance.

$$\frac{d\, \epsilon(t) C(t)}{dt} = -3\, k_v \rho_c \int_0^\infty n(L, t)\, G(L, t)\, L^2 dL \tag{12}$$

Multiplying the population balance (Eq. 2) by L^3 and integrating over size results in a relation for the change in void

fraction with time (De Wolf et al., 1989). Substitution of this relation simplifies Eq. 12 into:

$$\epsilon(t)\,\frac{d\,C(t)}{dt} = -3\,k_v[\rho_c - C(t)]\int_0^\infty n(L,\,t)\;G(L,\,t)\;L^2 dL \quad (13)$$

Fines are removed at the bottom of the outer draft tube, assuming a perfect separation at a cut size (L_{fi}). Their number after fines removal is given by:

$$\frac{n_{\text{after}}\,(L)}{n_{\text{before}}\,(L)} = \frac{Q_{\text{int1}}}{(Q_{\text{int1}} + Q_{fi})} \qquad L \leqq L_{fi} \quad (14)$$

The fines are readily dissolved and returned as solute. The increase in concentration after fines dissolution is given by:

$$C_{\text{after}} = C_{\text{before}} + \frac{\rho_c\,(1 - \epsilon_{fi})Q_{fi}}{\epsilon\,Q_{\text{int}}} \quad (15)$$

where

ϵ_{fi} = void fraction in the fines stream

Crystallizer internal: undersaturated

In an undersaturated slurry, the crystals will dissolve rather than grow. The growth rate G is, therefore, replaced by the dissolution rate DS using a different mass transfer coefficient, because the mass transfer coefficient for dissolution is given by the mass transfer coefficient for diffusion only.

$$\frac{\partial n(L,\,t)}{\partial t} + \frac{\partial[DS(L,\,t)\;n(L,\,t)]}{\partial L} = 0 \quad (16)$$

$$DS(L,\,t) = k_d(L)\,\frac{k_a}{3\,k_v\,\rho_c}\,C^*(t) + G_a(L,\,t) \quad (17)$$

$$C^*(t) = C_b(t) - C_s(T_1) \quad (18)$$

Concentration balance:

$$\epsilon(t)\,\frac{d\,C(t)}{d\,t} = -3\,k_v[\rho_c - C(t)]\int_0^\infty n(L,\,t)\;DS(L,\,t)\;L^2 dL \quad (19)$$

The growth regime will change into the dissolution regime only when the slurry is undersaturated. Whether or not this will occur depends on the initial supersaturation in the boiling zone, the increase in temperature in the internal heat exchanger, and the desupersaturation rate defined by Eq. 13. Equation 13 predicts that desupersaturation is promoted by a large crystal surface and high mass transfer rates. The effect of the occurrence of an undersaturated regime can be internal fines removal. Preferential fines dissolution is predicted by the mass transfer model given by Eq. 8 for equal driving forces. This mechanism probably acts as a source for crystallizer instability. Internal fines removal will reduce the specific surface area, which reduces the rate of desupersaturation. This continues until internal fines dissolving stops and a new cycle starts.

Simulation

A previously reported simulation technique, the method of lines (Jager et al., 1990a,b), was unstable, probably due to discontinuities in the growth rate, and therefore was rejected. Instead, another technique, according to a modified "fraction trajectory concept" (De Leer, 1981), which uses the method of characteristics, was used. Crystals born over a time interval (Δt) are collected in a size class with an average size (L_0^*).

$$N_0^* = B\,\Delta t \quad (20)$$

$$L_0^* = \tfrac{1}{2}\,G(L_0^*)\,\Delta t \quad (21)$$

where

$$B = k_b\,C^{*\,i}\,m_j^k \quad (22)$$

Subsequently, the average size in other size classes increases or decreases as a result of crystal growth or dissolution, the rate of which is defined by Eqs. 11 and 17.

$$\Delta L^*(x) = G[L^*(x)]\Delta t$$

or

$$\Delta L^*(x) = DS[L^*(x)]\Delta t \quad (23)$$

This results in a large number of size classes, unequally distributed along the size axis. Size classes below the nuclei size or size classes, which contain a minimal number of crystals, are discarded. The number of crystals in a size class remains constant in the crystallizer internals, because crystals are born or change in size only. Crystals are reduced in number if they are removed as the product in the boiling zone or removed as fines. In Eqs. 3, 10, 13 and 19, the number density distribution has to be integrated over size. For a discrete number distribution, the integral is given by:

$$m_j = \Sigma\,N(x)\;L(x)^j \quad (24)$$

The concentration balance is solved, similar to Eq. 23, by using the Heun integration technique. According to Kramer et al. (1990), the method of characteristics in the present form compares favorably with other techniques previously used in the simulation of mixed crystallizers. This fact supports its use in this application.

Results

A set of equations is solved numerically for a number of parameter combinations using a CSD, which was measured during the crystallizer start-up. The parameters for diffusive, convective mass transfer were chosen according to Eq. 25 (Jager, 1990), using a nuclei size of 5 μm.

$$k_d = \frac{5 \times 10^{-9}}{L} + 1.7 \times 10^{-4} \quad (25)$$

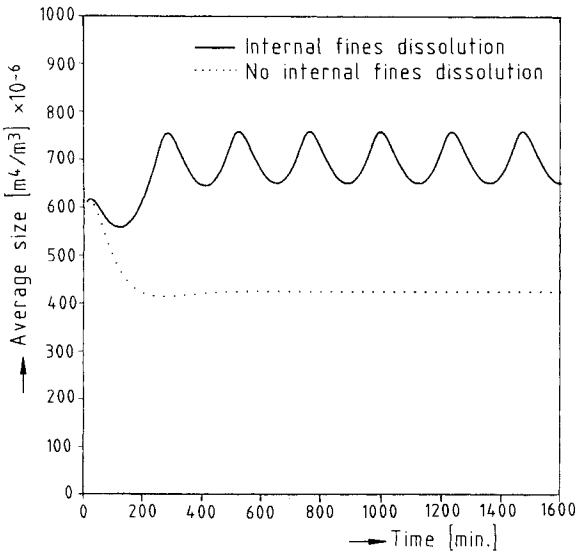

Figure 11. Simulated effect of internal fines dissolution on the mass-based average size during startup.

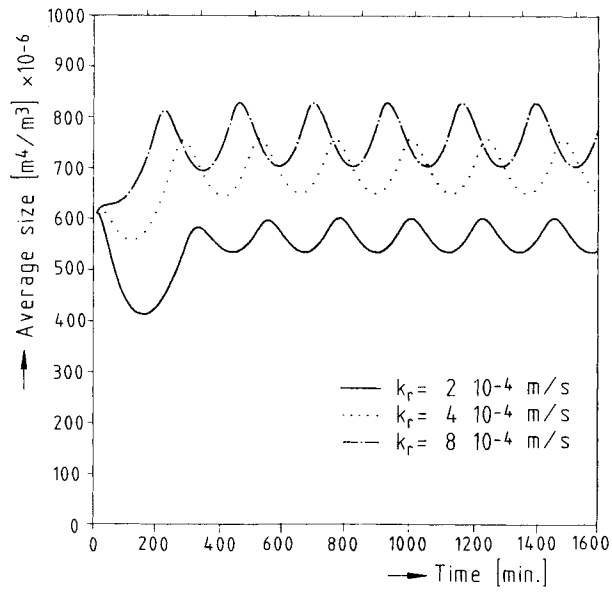

Figure 12. Simulated effect of changes in the reaction constant k_r on the mass-based average size during startup.

The reaction constant k_r was fixed at a value of 4.0 10^{-4} m/s in most graphs. A nucleation model was tentatively assumed (Jager et al., 1990a, b).

$$B(t) = k_b\, C^*(t)^{2.0}\, m_3(t) \tag{26}$$

The parameter k_b had a value of 9×10^8 to calculate an average size in the order of 700 μm, in accordance with the average size produced in the 970-L crystallizer. The rate of attrition is presented by:

$$G_a(L, t) = -1.5 \times 10^{-4}\, m_3(t)\ (L - 800 \times 10^{-6}) \tag{27}$$

The results presented here for an evaporative crystallizer will be limited to the operation without fines removal to show the effects of:

1. Internal fines removal
2. Change in the reaction constant k_r
3. Differences among a 20, 970 and 50,000-L scale of operation.

Internal fines removal

The effect of internal fines removal is eliminated by reducing the residence time in the inner draft tube to 0 s at the same total circulation time of 13 s. Resulting trends for the mass-based average size are presented in Figure 11, for a model both with and without inclusion of internal fines dissolution. These results indicate a significant decrease in the average size, when the effect of internal fines dissolution is neglected.

Growth kinetics

A change in growth kinetics will have a complicated impact. By increasing the resistance for crystal growth by decreasing the reaction constant k_r, crystal birth will be favored over crystal growth, and consequently the CSD will vary. As a result, the rate of desupersaturation will increase due to a larger surface area; however, this effect is counteracted by a decrease in the mass transfer coefficient for crystal growth k_r. Finally, the balance between crystal growth and dissolution predicted according to Eqs. 7, 8 and 18 will shift toward crystal dissolution. The trends for the mass-based average size for reaction constants of 2×10^{-4}, 4×10^{-4} and 8×10^{-4} m/s are presented in Figure 12.

Scale of operation

The model is solved for three crystallizer configurations: 20- and 970-L crystallizers presented in Part I of this article, and an imaginary 50,000-L crystallizer. The crystallizer dimensions are given in Table 1. The operating conditions are identical to the experimental conditions.

Figure 13 illustrates the resulting supersaturation profiles at the three scales of operation. These profiles are presented as supersaturation vs. time for a circulating lump of liquid. This is equivalent to the spatial variation of the supersaturation in the crystallizer. The stepwise changes in the supersaturation result from the assumption that the temperature changes stepwise. The trends of the corresponding mass-based average sizes are presented in Figure 14.

Simulated supersaturation profiles agree with the prediction made in Part I: the small-scale crystallizer has a flat supersaturation profile and no undersaturation, whereas the large

Table 1. Dimensions of Simulated Crystallizers

Vol. L	Height m	Dia. m	Cir. Time s	Cir. Rate m^3/s
20	0.5	0.2	2	0.010
970	2.7	0.7	13	0.0767
50,000	10.0	2.5	50	1.0

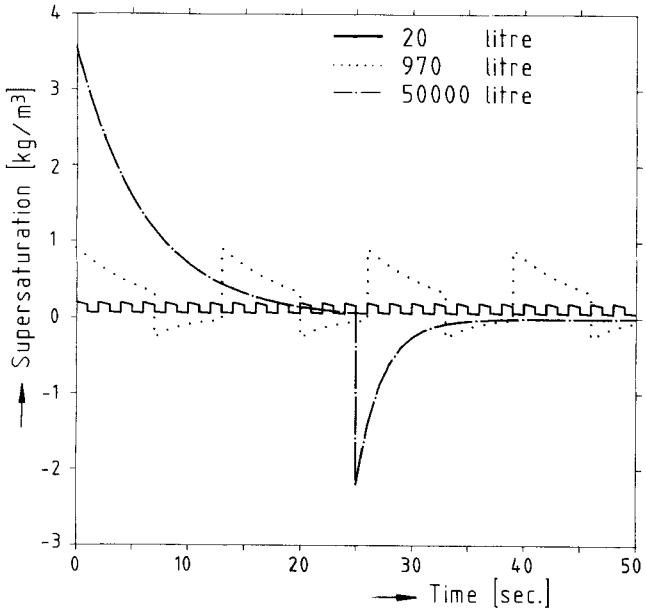

Figure 13. Typical supersaturation profiles.

Depicted as the variation of supersaturation vs. time for a circulating lump of liquid, which is equivalent to the spatial variation of the supersaturation for three crystallizers

crystallizer has a very steep profile and significant undersaturation.

In scale-up, the dynamic behavior of the mass-based average size changes dramatically, which is in line with the experimental findings and supports the conclusions drawn in Part I. The differences in steady-state values are related to the nucleation parameters chosen. In the large-scale crystallizer, internal fines removal will increase the average size of the crystals produced. In the small-scale crystallizer, the supersaturation is much lower, which benefits the crystal growth over the crystal birth,

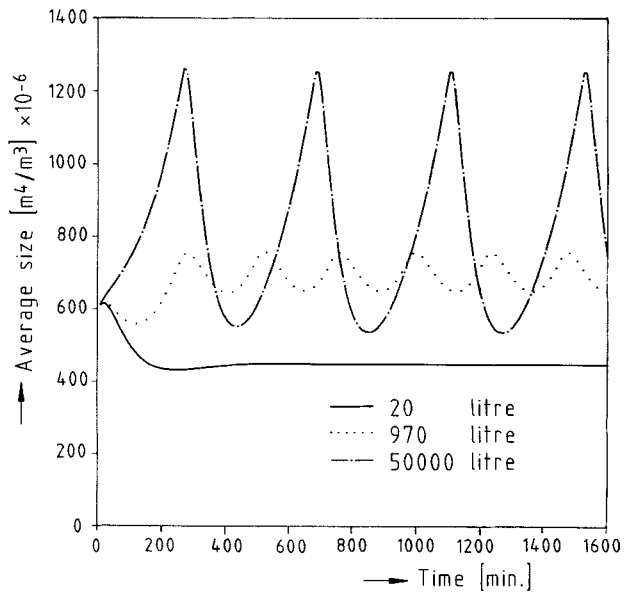

Figure 14. Mass-based average size for three scales of operation during crystallizer startup.

for a parameter i in the nucleation model exceeding one and which only partially compensates for the lack of internal fines removal. This can be seen by comparing the results for the 970-L crystallizer with and without account of internal fines removal with those for the 20-L crystallizer.

Although a number of parameter combinations were investigated, the numerical results obtained at this point only qualitatively predict the trends reported in Part I. They fail to quantitatively predict the cycle time and the decrease in amplitude in response to the 970-L crystallizer. The use of the parameter estimation technique presented by Jager et al. (1990a) was not pursued further. A manual variation of the parameters indicated room for limited improvement only at the cost of a large amount of computing power, since the model is very computationally-intensive. Furthermore, a measured size distribution is used as the initial condition, which introduces uncertain behavior during the start-up.

A closer look at the numerical results reveals, however, that there is a sharp size boundary, which shifts in time, beyond which crystals will dissolve or survive. Therefore, none of the new-born crystals will survive in a certain period of time. As a result, the CSD produced has sharp discontinuities, which are absent in the experimental data. It is well known that the nuclei produced have a size distribution (Garside et al., 1979), instead of being formed at one initial size. This refinement is insignificant for a large difference between the nuclei size and the average size in MSMPR models (Ramanarayanan et al., 1984). Preliminary results for the present model, however, have indicated that by using a nuclei size distribution instead of assuming nuclei of one initial size, the oscillations tend to be dampened (Jager, 1990). Therefore, optimization of the nuclei size distribution is certainly very important. However, without experimental data of the initial size distribution, this optimization is a formidable task.

Discussion

Without doubt, a supersaturation profile indeed exists in a large-scale crystallizer. The model is presented to simulate the effects of such a profile. The numerical results indicate the significant impact of the scale of operation of CSD dynamics, as a result of the difference in circulation time. This suggests that the kinetic data, obtained in small-scale crystallizers whose heights differ from large-scale equipment, cannot be used with certainty to predict CSD transients in a large-scale crystallizer without incorporating the significant effect of internal fines removal.

In the extended model, detailed information on nucleation, growth and attrition kinetics is required; however, this must partially be assumed since we have only limited knowledge so far. The effect of a supersaturation profile on the phenomenon of secondary nucleation is particularly unclear and certainly requires more research in the future. In this article, it is assumed that the rate of secondary nucleation is related directly to the local supersaturation. A second possibility would be to relate the nucleation rate to the supersaturation in the boiling zone because a large number of nuclei may have been initiated at the high supersaturation in the boiling zone. Additional research is also required to characterize the size distribution of the nuclei produced, because the size distribution of nuclei is probably important in representing the experimental data.

Conclusions

- The possibility to model CSD dynamics in more detail, using a reactor-engineering approach, has been illustrated. Such an approach can also be applied for other crystallizer geometries and for the study of precipitation processes where the effect of supersaturation profiles can be even more pronounced.
- The introduction of a supersaturation profile, as opposed to the general MSMPR assumption, significantly affects the predicted CSD dynamics, especially at a larger-scale of operation. The proposed model predicts oscillations at a larger-scale of operation, whereas dampened oscillations were observed experimentally. One possibility to predict the dampening of oscillations is to introduce nuclei with a size distribution instead of assuming them to form at one initial size.
- To model the CSD dynamics, detailed information on the nucleation kinetics is required. Since this information is not available currently, research on the secondary nucleation kinetics, especially in the presence of steep supersaturation profiles, should be given more emphasis.

Acknowledgment

The authors wish to thank the Netherlands Technology Foundation (STW), AKZO, DOW, DSM, DUPONT, RHONE POULENC, SUIKER UNIE, and UNILEVER for their financial support of the UNIAK research program. Ir. M. T. Oudkerk contributed to this article in his final year of the M.Sc. program.

Notation

a, b = empirical constants
B = nucleation rate, No./m^3·s
C = concentration, kg/m^3 clear liquor
C_b = concentration in the bulk of the liquid, kg/m^3 clear liquor
C_s = concentration at saturation, kg/m^3 clear liquor
C^* = supersaturation ($C_b - C_s$), kg/m^3 clear liquor
c_p = specific heat, kJ/kg·K
DS = rate of dissolution, m/s
g = acceleration of gravity, m/s^2
G = growth rate, m/s
G_a = rate of attrition, m/s
i, k = empirical constants
j = used to denote moments of the CSD
k_a = shape factor
k_b = nucleation constant
k_d = mass transfer coefficient for diffusion/convection, m/s
k_g = overall mass transfer coefficient for growth, m/s
k_r = mass transfer coefficient for surface integration, m/s
k_v = shape factor
L = crystal length, m
Msl = slurry density, kg/m^3 slurry
m_j = jth moment of the distribution
N = number of crystals, No./m^3 slurry
n_0 = population density at zero size, No./m^4
$n(L, t)$ = population density at size L, No./m^4
P = heat input, W
Q = flow rate, m^3/s
R = mass flux, kg/m^2·s
r = empirical constant
R_v = heat of evaporation, kJ/kg
t = time, s
T = temperature, K
V = crystallizer volume, m^3
x = index

Greek letters

$\Delta V(L_i, t)$ = volume fraction in the ith size class
ϵ = void fraction
ρ = density, kg/m^3
τ = residence time, s

indices

b = bulk
c = crystal
f = feed
if = interface
fi = fines
l = liquid
p = product
v = vapor
int1 = internal input flow
int2 = internal output flow
no index = crystallizer contents

Literature Cited

Aeschbach, S., and J. R. Bourne, "The Attainment of Homogeneous Suspension in a Continuous Stirred Tank," *Chem. Eng. J.*, **4**, 234 (1972).

Aeschbach, S., and J. R. Bourne, "The Influence of the Degree of Crystal Suspension on Crystallizer Stability," *Industrial Crystallization 78*, E. J. de Jong and S. J. Jancic, eds., North-Holland Publishing, Amsterdam, 259 (1979).

Beckman, J. R., and A. D. Randolph, "Crystal Size Distribution Dynamics in a Classified Crystallizer: II," *AIChE J.*, **23**, 510 (1977).

De Leer, B. G. M., "Draft-Tube-Baffle Crystallizers," PhD Thesis, Delft Univ. of Technology (1981).

De Wolf, S., J. Jager, H. J. M. Kramer, R. Eek, and O. H. Bosgra, "Derivation of State Space Models of Continuous Crystallizers," *Proc. IFAC Symp. on Dynamics and Control of Chemical Reactors*, Maastricht, 107 (1989).

Garside, J., I. T. Rusli, and M. A. Larson, "Origin and Size Distribution of Secondary Nuclei," *AIChE J.*, **25**, 57 (1979).

Grootscholten, P. A. M., and E. J. de Jong, "The Influence of Supersaturation Rate Decay on the Design of Industrial Evaporative Crystallizers," IChemE Meeting, University College, London (1979).

Grootscholten, P. A. M., L. D. M. van de Brekel, and E. J. de Jong, "Effect of Scale-Up on Secondary Nucleation Kinetics for the Sodium Chloride-Water System," *Chem. Eng. Res. Des.*, **62**, 179 (1984).

Jager, J., "Control of Industrial Crystallizers," PhD Thesis, Delft Univ. of Technology (1990).

Jager, J., S. de Wolf, H. J. M. Kramer, and E. J. de Jong, "Estimation of Nucleation Kinetics from CSD Transients of a Continuous Crystallizer," *Chem. Eng. Sci.*, accepted (1990a).

Jager, J., S. de Wolf, H. J. M. Kramer, and E. J. de Jong, "Estimation of Nucleation and Attrition Kinetics from CSD Transients of a Continuous Crystallizer," *Chem. Eng. Res. Des.*, accepted (1990b).

Jager, J., S. de Wolf, H. J. M. Kramer, and E. J. de Jong, "On-Line Particle Size Measurement in Dense Slurries," *Powder Technol.*, **62**, 155 (1990c).

Kramer, H. J. M., S. de Wolf, and J. Jager, "Simulation of the Dynamic Behaviour of Continuous Crystallizers," *Crystallization As a Separations Process*, A. S. Myerson and K. Toyokura, eds., ACS, Washington, DC, 159 (1990).

Kratz, E., and F. Hoyer, "Scale-Up from Pilot-Plant Test Data: a Simplified Numerical Approach," *Industrial Crystallization 87*, J. Nyvlt and S. Zacek, eds., Elsevier, Amsterdam, 319 (1989).

Ottens, E. K., "Nucleation in Continuous Agitated Crystallizers," PhD Thesis, Delft Univ. of Technology (1973).

Ramanarayanan, K. A., K. Athreya, and M. A. Larson, "Statistical-Mathematical Modeling of CSD in Continuous and Batch Crystallizers," *AIChE Symp. Ser.*, **80**, 76 (1984).

Randolph, A. D., J. R. Beckman, and Z. I. Kraljevich, "Crystal Size Distribution Dynamics in a Classified Crystallizer: I," *AIChE J.*, **23**, 500 (1977).

Randolph, A. D., and M. A. Larson, "Theory of Particulate Processes," Academic Press, San Diego (1988).
Riviera, T., and A. D. Randolph, "A Model for the Precipitation of Pentaerythritol Tetranitrate," *Ind. Eng. Chem. Process Des. Dev.*, **17**, 182 (1978).
Song, Y. H., and J. M. Douglas, "Self-Generated Oscillations in Continuous Crystallizers: II," *AIChE J.*, **21**, 924 (1975).
Wiker, S. L., and B. E. Anshus, "The Characteristics of a Non-isothermal Loop Crystallizer," *Chem. Eng. Sci.*, **29**, 1575 (1974).
Yu, K. M., and J. M. Douglas, "Self-Generated Oscillations in Continuous Crystallizers: I," *AIChE J.*, **21**, 917 (1975).

Appendix: Derivation of Mass and Heat Balances in the Boiling Zone

The different flows using the following notation are illustrated in Figure 9:

Q_f = feed flow
Q_p = product flow
Q_v = vapor flow
Q_{fi} = fines flow
$Q_{\text{int.1}}$ = internal input flow
$Q_{\text{int.2}}$ = internal output flow

Assumptions:

1. The crystallizer volume is constant.
2. The crystallizer temperature after evaporation is constant.
3. The heat is supplied in the internal heat exchanger only.
4. The boiling zone has a negligible volume and acts as a flow splitter only.
5. The density of the liquid and the saturation concentration change with temperature only, and other physical properties are assumed constant.
6. The heat of crystallization is negligible.

Heat balances:

heat input (feed + internal) = heat output (internal + product + vapor)

$$Q_f\rho_f c_{p1}T_f + Q_{\text{int.1}}[\epsilon_1\rho_1 c_{p1} + (1 - \epsilon_1)\rho_{c1}c_{pc}]T_1 = Q_{\text{int.2}}[\epsilon_2\rho_1 c_{p1} + (1 - \epsilon_2)\rho_{c1}c_{pc}]T_2 + Q_p[\epsilon_2\rho_1 c_{p1} + (1 - \epsilon_2)\rho_{c1}c_{pc}]T_2 + Q_v(\rho_v c_{pv}T_2 + \rho_v R_v) \quad \text{(A1)}$$

internal heat input =

$$Q_{\text{int.2}}[\epsilon_2\rho_1 c_{p1} + (1 - \epsilon_2)\rho_{c1}c_{pc}]T_2 - Q_{\text{int.1}}[\epsilon_1\rho_1 c_{p1} + (1 - \epsilon_1)\rho_{c1}c_{pc}]T_1 \quad \text{(A2)}$$

Mass balances:

The total mass balance is given by:

mass input (feed + internal) = mass output (internal + product + vapor)

$$Q_f\rho_f + Q_{\text{int.1}}[\epsilon_1\rho_1 + (1 - \epsilon_1)\rho_c] = Q_{\text{int.2}}[\epsilon_2\rho_1 + (1 - \epsilon_2)\rho_c] + Q_p[\epsilon_2\rho_1 + (1 - \epsilon_2)\rho_c] + Q_v\rho_v \quad \text{(A3)}$$

The internal mass balance is given by:

$$Q_{\text{int.1}}[\epsilon_1\rho_1 + (1 - \epsilon_1)\rho_c] = Q_{\text{int.2}}[\epsilon_2\rho_1 + (1 - \epsilon_2)\rho_c] \quad \text{(A4)}$$

The solute balance is given by:

$$Q_{\text{int.1}}\epsilon_1 C_1 + Q_f C_f = Q_{\text{int.2}}\epsilon_2 C_2 + Q_p\epsilon_2 C_2 \quad \text{(A5)}$$

The crystal mass balance is given by:

$$Q_{\text{int.1}}(1 - \epsilon_1)\rho_c = Q_{\text{int.2}}(1 - \epsilon_2)\rho_c + Q_p(1 - \epsilon_2)\rho_c \quad \text{(A6)}$$

The unknown variables ϵ_2 and $Q_{\text{int.2}}$ can be calculated iteratively for given values of ϵ_1 and $Q_{\text{int.1}}$ using Eqs. A4 and A6. Unknown variables Q_f, Q_v, T_2, and C_2 can then be calculated using the known variables Q_p, T_1, C_1 and known material properties using Eqs. A1, A2, A3 and A5.

Manuscript received June 21, 1990, and revision received Nov. 27, 1990.